Journal of Drug Delivery Science and Technology 70 (2022) 103206

Contents lists available at ScienceDirect

Journal of Drug Delivery Science and Technology

journal homepage: www.elsevier.com/locate/jddst

Opinion paper

Design and physicochemical characterization of novel hybrid SLN-liposome nanocarriers for the smart co-delivery of two antitubercular drugs

Eleonora Truzzi [a], Angela Capocefalo [b], Fiorella Meneghetti [c], Eleonora Maretti [a], Matteo Mori [c], Valentina Iannuccelli [a], Fabio Domenici [d,***], Carlo Castellano [e,**], Eliana Leo [a,*]

[a] Department of Life Sciences, University of Modena and Reggio Emilia, via G. Campi 103, Modena, Italy
[b] Institute for Complex Systems (ISC-CNR), National Research Council, Rome, Italy
[c] Department of Pharmaceutical Sciences, University of Milan, via L. Mangiagalli 25, Milan, Italy
[d] Department of Chemical Science and Technologies, University of Rome Tor Vergata, via Della Ricerca Scientifica, Rome, Italy
[e] Department of Chemistry, University of Milan, via C. Golgi 19, Milan, Italy

ARTICLE INFO

Keywords:
SANS
AFM
Nanoparticles
Rifampicin
Isoniazid

ABSTRACT

In the present work a novel hybrid system for the delivery of two first-line antitubercular drugs, rifampicin (RIF) and isoniazid (INH), was designed. In order to control the release of the drugs and improve the efficiency of conventional carriers, like liposomes or solid lipid nanoparticles (SLNs), the new systems were developed by embedding SLNs into lecithin-based liposomes through the reverse-phase evaporation method. The hybrid system was characterized and compared to SLNs and liposomes in terms of size, encapsulation efficiency, morphology, and drug release. Detailed structural data and further evidence of the successful formation of the hybrid nanoparticles were obtained by applying small-angle neutron scattering (SANS). The hybrid system displayed a particle size comparable to liposomes and a high encapsulation efficiency. Morphological results obtained by atomic force microscopy (AFM) highlighted the possible presence of SLNs into the phospholipid bilayer; this hypothesis was supported by the slower *in vitro* release of the hydrophilic drug INH compared to liposomes and SLNs. Moreover, scattering differences of the inner core of the nanoparticles, evidenced in the SANS analysis, further corroborated the successful formation of the hybrid carrier. These novel systems were able to release their content as expected from an efficient dosage form in a perspective of an inhaled administration, improving the stability and the drug release profile with respect to plain liposomes. The physicochemical characterization of our systems opens new avenues towards a better understanding of the formulation of vesicles encapsulating SLNs.

1. Introduction

The treatment of lung infections represents one of the great challenges of our time. These conditions are caused by a variety of bacterial, viral, and fungal agents, including *Mycobacterium tuberculosis* and, more recently, SARS-COV2. Tuberculosis (TB) still ranks as the first cause of death from a single pathogen, and the Covid-19 pandemic threatens to reverse the progress made in the last years in terms of diagnosis and disease control.

Pulmonary drug delivery of nanoparticle-based therapeutics have emerged as promising strategy, allowing the improvement of the pharmacokinetic profile and therapeutic efficiency of drugs, compared to conventional delivery systems [1,2]. In this context, inhaled therapy by lipid nanoparticles offers great benefits [3]. Solid lipid nanoparticles (SLNs) are monophasic structures formed by biocompatible lipids and a hydrophilic surfactant layer that keeps them in suspension. The main advantage of SLNs is their excellent physicochemical stability, which provides greater protection against the degradation of labile drugs [4]. In the last decade, SLNs have been demonstrated to be an effective drug delivery system for *anti*-TB inhaled therapy [5–8]. Despite their advantages, SLNs are characterized by a low drug loading capacity and rapid release, especially when hydrophilic drugs are concerned.

* Corresponding author.
** Corresponding author.
*** Corresponding author.
E-mail addresses: fabio.domenici@uniroma2.it (F. Domenici), carlo.castellano@unimi.it (C. Castellano), eliana.leo@unimore.it (E. Leo).

https://doi.org/10.1016/j.jddst.2022.103206
Received 6 October 2021; Received in revised form 3 February 2022; Accepted 22 February 2022
Available online 24 February 2022

Liposomes are spherical vesicles, formed by an aqueous core surrounded by bilayers of phospholipids, which can be exploited to transport both hydrophilic and lipophilic drugs through the respiratory tract [9]. Due to their high biocompatibility and easy aerosolization, liposomes represent one of the most promising drug delivery systems for the treatment of pulmonary infections [10,11].

Hybrid particles, composed by SLNs embedded in liposomes, were designed to obtain a new multi-compartmental drug delivery system. In detail, the lipid bilayer of liposomes was predicted to increase the colloidal stability and efficiency of intracellular delivery of the resulting hybrid system, while the nanoparticulate cores were employed to improve the pharmaceutical performance of liposomes. Moreover, the use of no additional chemical components allowed to avoid the risk of toxicity.

Rifampicin (RIF) and isoniazid (INH) are two first-line *anti*-TB agents, which are part of the standard treatment regimen for drug-susceptible TB. Recently, their co-administration (Rifinah®) has been shown to improve the clinical outcomes of TB patients [12]; in this context, the use of nanocarriers could enhance the pharmacokinetic properties of this combination, ensuring greater efficacy [13].

Our preliminary results showed that SLNs were unable to achieve an effective, durable encapsulation of the two drugs (INH, LogP −0.64; RIF, LogP 3.719) [14,15]. In particular, INH, owing to its hydrophilic nature, was rapidly released from the lipid matrix. Therefore, hybrid systems, generated by using liposomes as templates for the deposition of SLNs, were developed for the co-delivery of the two antitubercular drugs.

First, to formulate the hybrid nanocarriers we optimized the composition and the experimental parameters in preliminary studies. Then, because the successful implementation of a particle-based delivery system requires a detailed understanding of the morphology and properties of the drug carrier, the newly developed hybrid SLN-liposomes were characterized by Photon Correlation Spectroscopy (PCS), atomic force microscopy (AFM), and small-angle neutron scattering (SANS). In our previous work, we demonstrated that SANS is a powerful tool for the investigation of amphiphilic aggregates, such as liposomes [9]. SANS experimental data allowed us to characterize our nanoparticles in terms of overall size, dimension of the aqueous core and thickness of the lipid shell Moreover, it was useful to obtain indications on the localization of the drugs in the nanoparticles, through a comparison between loaded and unloaded systems within the same carrier category.

Finally, *in vitro* drug release studies were performed to gather key information on the newly developed nanoparticles in terms of effectiveness of the drug release profile.

Our results will aid researchers in the selection of the appropriate carrier based on the drug chosen in therapy, and in addressing the remaining challenges that need to be overcome to enhance the efficiency of current pulmonary delivery systems.

2. Materials and methods

2.1. Materials

Regarding the preparation of SLNs, mono-, di-, and triglycerides of Behenic acid (Compritol ATO 888) were a kind gift from Gattefossè (Saint Priest, Cedex, France); Tween 80 was purchased from Sigma-Aldrich (Milano, Italy). For the preparation of liposomes, Cholesterol 95% was purchased from Acros (Geel, Belgium) and soy Lecithin from Farmalabor (Canosa di Puglia, Italy). Rifampicin (RIF) was kindly gifted from Sanofi (Brindisi, Italy), while Isoniazid (INH) was purchased from T.C.I. Europe (Zwijndrecht, Belgium); these compounds were used as drug models for all the formulations. Milli-Q water was obtained from a Millipore system (Bedford, MA, USA). Deuterated 1,3-distearoyl-2-oleoyl glycerol was purchased from Toronto Research Chemicals (Toronto, Canada), and D_2O from VWR (Milan, Italy).

All employed solvents were of analytical grade.

2.2. Drugs-excipients compatibility

2.2.1. Infrared spectroscopy

The attenuated total reflectance-Fourier transform infrared (ATR-FTIR) spectra of pure materials (RIF, INH, Compritol, cholesterol, lecithin), and their physical mixtures (PMs) were acquired using a Spectrum Two FT-IR spectrometer equipped with a Universal ATR sampling accessory (PerkinElmer, Milano, Italy). The PMs were prepared by mixing the pure materials/drugs at the same ratio as the final formulations. The spectra were obtained in the spectral range 4000–450 cm^{-1} with a spectral resolution of 4 cm^{-1}, averaging 4 scans per spectrum. The background spectrum of the empty ATR diamond cell was acquired prior to each analysis under the same instrumental conditions. Finally, the spectra were subjected to baseline correction.

2.2.2. Differential scanning calorimetry and thermogravimetric analysis

Individual components (RIF, INH, Compritol, cholesterol, lecithin) and the ternary physical mixtures (PMs) prepared at the same pure materials/drugs ratio as the formulation, were also analyzed also using simultaneous thermogravimetry and differential scanning calorimetry (TG/DSC) (NETZSCH mod. 429CD, Netzsch-Gerätebau GmbH, Selb, Germany). The selected temperature range used was 20–300 °C with a heating gradient of 10 °C/min. The analyses were performed in triplicate.

2.3. Nanocarrier preparation

2.3.1. SLNs preparation

The melt-emulsification procedure was used to obtain co-loaded SLNs with a drug/excipient weight ratio of 1:2. Briefly, the lipid phase including 60 mg of Compritol (with 15 mg of INH and 15 mg of RIF in co-loaded particles) was melted at 85 °C, and then emulsified at the same temperature in 3 mL of Tween 80 aqueous solution (1.7% w/v) by ultrasonication for 1 min, at 20 W (Vibra-Cell, Sonics&Materials, NewTown, CT, USA). The subsequent step of homogenization was carried out using an Ultra-Turrax instrument (Ika-euroturrax T 25 basic, IkaLabortechnik, Staufen, Germany) at 24,000 rpm for 1 min (T-25 basic, Ika Labortecnik, Germany). Finally, the O/W emulsion was further ultrasonicated in the same conditions. Then, the emulsion was cooled in an ice-bath and purified three times by centrifugation at 6000×*g* for 30 min (Rotina 380R, Hettich, Germany) in 100 kDa MWCO Vivaspin columns (Sartorius, Goettingen, Germany). The samples were diluted with deionized water to a volume of 3 mL and used for the preparation of SLN-loaded liposomes.

For the determination of drug loading in the plain SLNs, the use of chloroform was required to dissolve the lipid matrix of the Compritol. In order to facilitate the dissolution of Compritol in chloroform, the analysis was carried out on the freeze-dried formulation, obtained without adding cryoprotectants. The freeze-drying process was performed at −55 °C at a pressure of 10^{-4} Torr for 24 h (Lio 5P, Cinquepascal, Milan, Italy). Then, the samples were stored as dry powder at 25 °C and used in the *in vitro* assays.

For the SANS experiments, deuterated 1,3-distearoyl-2-oleoyl glycerol (2 mg) was used in combination with Compritol.

2.3.2. Liposome preparation

Co-loaded Liposomes were prepared by Reverse Phase Evaporation (REV), as previously reported [9], using a drug/excipient weight ratio of 1: 3.3. Briefly, Cholesterol (Chol) and soy lecithin were solubilized in chloroform at a fixed molar ratio (1:1, with 15 mg RIF for co-loaded liposomes), were solubilized in chloroform reaching a final concentration of 40 mM. Thereafter, the solution was put into a round-bottom flask, removing the solvent under vacuum at room temperature, until a dry film was obtained (Buchi HB-140, Buchi, Switzerland). The film was re-dissolved in diethyl ether and then mixed with 3 mL of water (containing 15 mg of INH for co-loaded samples), with a 3:1 vol ratio of

ether to water. The suspension was vortexed for 3 min to form a W/O emulsion. The resulting emulsion was stirred for 2 h at 200 rpm to remove the organic solvent, thus inducing the phase reversal and, finally, the formation of liposomes. The latter were homogenized by Ultra-Turrax (Ika-euroturrax T 25) for 3 min and purified by dialysis for 30 min to separate the free drugs, before being transferred to vials and stored at 4 °C.

For the SANS investigation, liposomes were prepared and purified using D_2O instead of Milli-Q water.

2.3.3. Hybrid SLN-liposome preparation

Hybrid SLN-liposomes were prepared following the procedure previously reported for liposomes and by using 3 mL of unloaded or co-loaded SLN suspension, instead of water for the preparation of the W/O emulsion with diethyl ether. For these systems, the drug/excipients weight ratio was 1: 5.3. The hybrid SLN-liposomes were purified by 30 min dialysis and then stored at 4 °C.

For the SANS analysis, hybrid SLN-liposomes were prepared with SLNs composed by deuterated 1,3-distearoyl-2-oleoyl glycerol (2 mg), and D_2O instead of Milli-Q water.

2.4. Particle size and Z-potential

Particle size (average hydrodynamic diameter by intensity together with polydispersity index, PDI) and Z-potential were determined by photon correlation spectroscopy (PCS), using a Zetasizer Nano ZS analyzer system (Zetasizer version 6.12; Malvern Instruments, Worcs, U. K.). Each experiment was carried out at 25 °C using deionized water with a refraction index of 1.33, a viscosity of 0.8872 cP, using a fixed angle at 90°. The results in triplicate were the average of three different measurements. Each measurement was the average of at least 12 runs.

2.5. Atomic force microscopy (AFM)

The morphology of SLNs, liposomes, and hybrid SLN-liposomes was obtained by atomic force microscopy (AFM). AFM measurements were performed by a Multimode system endowed with a Nanoscope 3D controller (Bruker, Karlsruhe, Germany). Topographic and phase images were acquired in non-contact mode, at room temperature (20 °C) and atmospheric pressure. Immediately before the analysis, freshly prepared unloaded samples (SLNs, liposomes, and hybrid particles), already diluted in water (1:100 v/v), were deposited onto a 1 cm diameter mica disk. After 3 min, the excess of water was removed and the collected AFM images were analyzed by Gwyddion (2.5 version) software.

2.6. Drug loading and encapsulation efficiency

Encapsulation efficiency (EE %) and drug loading (DL %) of SLNs, liposomes, and hybrid SLN-liposomes were estimated by UV–visible spectroscopy (Lambda 3B Perkin-Elmer, Waltham, MA, USA). The standard calibration curves allowed the conversion of the absorbance of the solution to the amount of drug contained in the sample. The calibration curves were obtained by measuring the supernatants of the corresponding unloaded samples (n = 6), in order to remove any possible interference in the measurements.

The straight quantification of RIF and INH in co-loaded nanocarriers could not be accomplished in a simple way by UV–visible spectroscopy, due to the overlapping of the absorption spectra of RIF at the INH absorption peak (262 nm) of the absorption spectra of RIF [14].

Therefore, first-order derivative UV spectroscopy at 249 nm was used to determine INH, while the original UV absorption spectrum was adopted to determine RIF, at 475 nm. The reliability of derivative UV spectrophotometry for the simultaneous estimation of INH and RIF was proved by Gürsoy et al. [15]. Original and first-order derivative spectra of RIF and INH are reported in the supplementary materials.

DL % and EE % were calculated by using the following equations:

$$DL\% = \frac{incorporated\ drug\ (mg)}{total\ mass\ of\ sample^{*}\ (mg)} \times\ 100$$

$$EE\% = \frac{incorporated\ drug\ (mg)}{initial\ drug\ (mg)}\ x\ 100$$

* Weighed after freeze-drying.

2.6.1. SLN drug loading determination

For the content determination of INH in SLNs, 10 mg of freeze-dried SLNs were dissolved in 1 mL of chloroform; then, 5 mL of Milli-Q water were gradually added in portions of 1 mL, mixing by vortex for 1 min after each addition to extract the drug. The mixture was centrifuged (Rotina 380R, Hetting, Germany) for 30 min at 9500×*g* to separate the two phases, and the aqueous supernatant containing the hydrophilic drug was analyzed using a UV–visible spectrophotometer (first-order derivative) at 249 nm (Lambda 3B Perkin-Elmer, Waltham, MA, USA).

For the determination of RIF, 10 mg of freeze-dried SLNs were dissolved in 1 mL of chloroform, and then 4 mL of methanol (MeOH) were added. The obtained solution was vortexed for 2 min. After centrifugation (10 min at 9500 g), to separate potential undissolved lipids, RIF was quantified in the solution by spectrophotometry, recording the absorbance at 475 nm.

2.6.2. Liposome and hybrid SLN-liposome drug loading determination

To determine INH loading, 300 μL of liposomal suspension was dissolved in 1.5 mL of isopropanol (IPA), and then Milli-Q water (5.2 mL) was added. For the determination of RIF loading, 300 μL of liposomal suspension was dissolved in 1.5 mL of IPA, and then 5.2 mL of MeOH was added. In both cases, the drug loading was spectrophotometrically calculated in the respective solutions, as described in paragraph 2.5.

The procedure used for plain liposomes was also adopted for hybrid SLN-liposomes, with a slight variation: after adding IPA, the mixture was heated at 85 °C for 10 min to completely melt the SLNs before the extraction of INH and RIF by water or MeOH, respectively. The quantification was achieved as described in section 2.6.

2.7. SANS analysis

SANS experiments were performed by the time-of-flight instrument V16 at the Helmholtz-Zentrum Berlin (HZB, Berlin, Germany). A range of scattering vector $q = (4\pi/\lambda)\ \sin\theta$ (where λ is the neutron wavelength and 2θ is the scattering angle) between 0.0035 $Å^{-1}$ and 0.07 $Å^{-1}$ was explored through neutron wavelengths spanning from 2 Å to 9 Å, with a 2 m and 11 m sample-detector distance, respectively. The samples were measured in 2 mm path length quartz cuvettes of UV-spectrophotometer-grade, located on an enclosed, computer-controlled sample chamber. The scattering data were normalized for the sample transmission, the background was corrected with the signal of the solvent (D_2O), and the component of the instrumental smearing (*i.e.*, detector linearity and efficiency response) was taken into account. Data reduction was performed using the software package MantidPlot [16].

Experimental data were analyzed by the core-shell spherical model of the fitting routine SASView 5.0.3, in the context of a spherical core-shell morphology for both liposomes and SLNs. The employed model provides the form factor *P(q)* for non-interacting spherical particles with a core-shell structure [17]:

$$P(q) = \frac{x}{V_p}\left[3V_c(\rho_c - \rho_s)\frac{\sin qr_c - qr_c\cos qr_c}{(qr_c)^3} + 3V_r(\rho_s - \rho_0)\frac{\sin qr_p - qr_p\cos qr_p}{(qr_p)^3}\right]^2$$

where x is a scale factor, V_p is the volume of the core-shell sphere with radius r_p, V_C is the volume of the particle's core, r_c is the radius of the core, ρ_c and ρ_s are the scattering length densities (SLDs) of the core and of the shell, respectively, and ρ_0 that of the solvent. The shell thickness t

is obtained by $t = r_p - r_c$.

2.8. In vitro drug release studies

The *in vitro* release of RIF and INH from SLNs, liposomes, and hybrid SLN-liposomes was determined in Simulated Lung Fluid (SLF) at pH 7.4 [18]. A definite amount of sample (45 mg of freeze-dried SLNs suspended in 1 mL of deionized water or 1 mL of liposomal dispersions) was put into a dialysis membrane (Dialysis Tubing – Visking MWCO-12-14000 Da, Medical International Ltd, London). The dialysis tube was immersed into a vessel containing 30 mL of SLF medium and maintained at 37 ± 0.5 °C, under gentle stirring. At fixed times, aliquots (1 mL) were removed from the solution, and the INH and/or RIF content was determined by spectrophotometric analysis. For each time point, two aliquots were analyzed using unloaded carriers as blank samples; the study was performed in triplicate. INH and RIF were quantified by spectrophotometry, as described in section 2.5.

2.9. Statistical analysis

Statistical comparison of drug content was performed by one-way Analysis of Variance (ANOVA) test, followed by a Tukey's test. Differences between groups were considered statistically significant at $p < 0.05$.

3. Results

3.1. Drug-excipient compatibility

ATR-FTIR spectroscopy was employed to assess the compatibility of the excipients employed in the formulation of the carrier. The spectra of the pure drugs (RIF and INH), Compritol (used in the formulation of SLN), and their PMs are displayed in Fig. 1, while the spectra of the individual spectra of the excipients used in the liposome formulation (lecithin, cholesterol), along with the two drugs and their PMs are displayed in Fig. 2.

Compritol (glycerol dibehenate) showed typical bands related to the aliphatic chain of the saturated fatty acids and glycerol moiety. In particular, the most intense peaks were induced by the symmetric and antisymmetric C–H stretching of $–CH_2$ and $–CH_3$ groups of fatty chains at 2916 and 2848 cm^{-1}. The other representative signals at 1735, 1467, 1175, and 719 cm^{-1} were attributed to C=O stretching, methylene C–H bend, skeletal C–C vibrations, and methylene $–(CH_2)_n$ rocking respectively. The lipophilic drug RIF was characterized by several intense peaks in the fingerprint region, especially related to the C=C–C and C–H aromatic ring stretch and bend, C–O alcoholic stretch, C–N and = N–H stretch of the imino and tertiary amino groups [19]. The FTIR spectrum of pure INH showed characteristic peaks of conjugated carbonyl C=O bond (1662 cm^{-1}), amino group NH_2 (1330 cm^{-1}), N–N single bond (1220 cm^{-1}), N–H bending (1554 cm^{-1}), and C–C=O bending (670 cm^{-1}) [20]. The PM exhibited the same signals as the Compritol without any shift.

Cholesterol showed characteristic peaks related to the secondary alcohol at 3433 and 1051 cm^{-1} for O–H and C–O stretching respectively. Being predominantly composed of saturated aliphatic saturated groups, the other peaks were typical of CH_3, CH_2, and CH vibrations. Lecithin, being a phospholipid mixture, exhibited characteristic signals at 1736 cm^{-1} for C=O stretching and in the region between 1224 and 974 cm^{-1} related to the phosphate group in the spectrum. Furthermore, the choline moiety of the phosphatidylcholine generated the signal at 974 cm^{-1} induced by the $C–N^+–C$ asymmetric stretch. The remaining peaks corresponded to the fatty acid chains vibrations. Both the PMs exhibited the same signals as lipids, without any additional vibration or peak shift induced by the two drugs.

The TGA data reported in each image of Fig. 3 showed in all the cases (individual drugs, excipients, and ternary PMs) a mass loss in the range of 190–250 °C range. Regarding thermal analyses, the DSC curve of RIF showed two exothermic peaks at about 200 °C and 247 °C (Fig. 3a), while that of INH exhibited a single endotherm at about 178 °C (Fig. 3b). The typical peak of Compritol, the lipid used for SLNs preparation, was observed at 78 °C (Fig. 3c). The corresponding ternary PM (Fig. 3d) presented two peaks at about 74 °C and 165 °C for Compritol and INH, respectively, with a mild reduction in the Tm compared to the thermogram of the pure materials. No peak referable to RIF was detected. The curves related to cholesterol and lecithin showed a peak at about 150 °C for cholesterol (Fig. 3e) and at 180 °C for lecithin (Fig. 3g). The two ternary PMs presented the characteristic peaks of the two excipients, cholesterol in Fig. 3f and lecithin in Fig. 3h, as well as a clearly visible peak belonging to INH peak clearly visible and a hinted peak attributable to RIF peak. Good compatibility between drugs and excipients was also confirmed also by DSC for both SLNs and liposomes. Moreover, the absence of the characteristic RIF peak in the PMs with Compritol indicates that RIF can be embedded in the lipid matrix in an amorphous state.

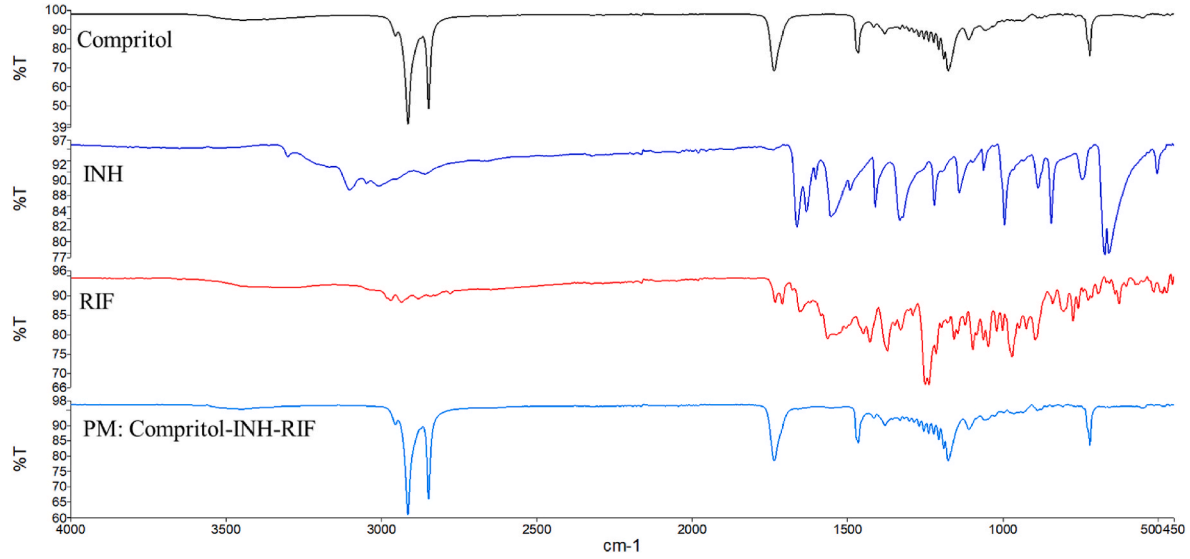

Fig. 1. Attenuated total reflectance-Fourier transform infrared (ATR-FTIR) spectra of Compritol, isoniazid (INH), rifampicin (RIF), and their ternary physical mixture composed by the lipid and the two drugs (PM).

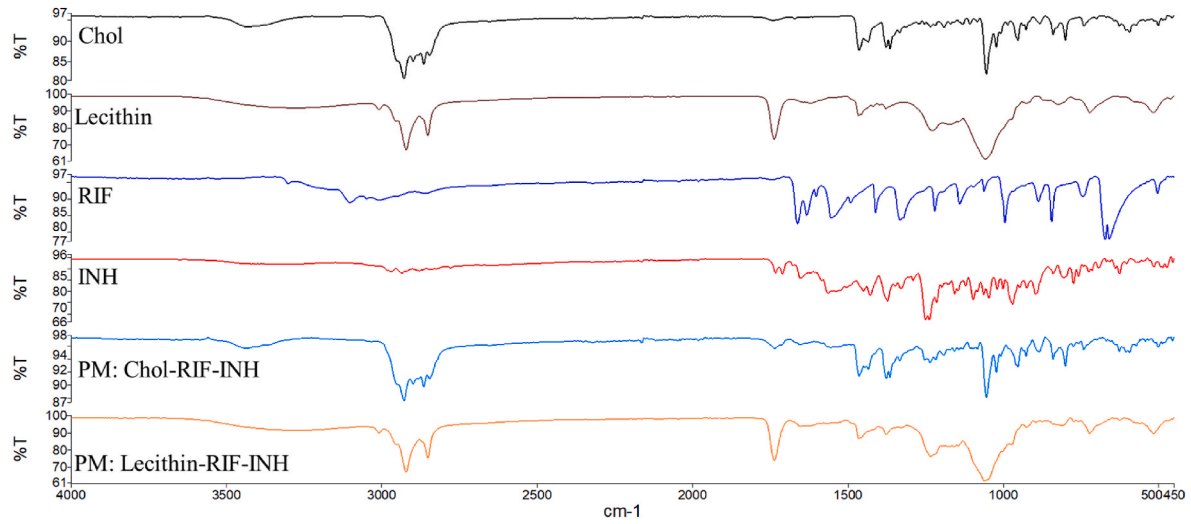

Fig. 2. Attenuated total reflectance-Fourier transform infrared (ATR-FTIR) spectra of lecithin, cholesterol, isoniazid (INH), rifampicin (RIF), and their ternary physical mixtures composed by each lipid and the two drugs.

3.2. SLNs, liposomes, and hybrid SLN-liposomes characterization

In this study, a hybrid system was designed to obtain a novel nanocarrier offering an improved encapsulation efficiency and controlled release of the embedded drugs.

Size, polydispersity index (PDI), and Z-potential, determined by PCS analysis, as well as encapsulation efficiency (EE%) and drug loading (DL % w/w) of the analyzed samples are summarized in Table 1.

SLNs had a small size (about 130 nm), with a homogenous size distribution (PDI <0.3), while liposomes were bigger (300 nm) and non-homogeneous in size, with a higher PDI value, indicating a multimodal particle distribution. No significant differences in size could be appreciated between liposomes and hybrid SLN-liposomes, neither for the unloaded nor for the co-loaded samples. The size homogeneity of liposomes seemed to decrease with the incorporation of SLNs into the liposomal bilayer, considering that the PDI for hybrid SLN-liposomes was >0.4. With respect to the Z-potential, which describes the surface particle charge, the values for all the co-loaded samples were considerably more negative compared to those of the unloaded samples.

Hence, we can conclude that we successfully obtained nanoscale devices, with a particle size within the suitable range for pulmonary delivery.

The main rationale behind the design of this hybrid carrier was to improve the encapsulation and/or release kinetics of hydrosoluble drugs. The EE% for the lipophilic drug RIF in conventional SLNs and liposomes was comparable, while for the hydrophilic drug INH the EE% was significantly lower in the case of SLNs. Despite hybrid SLN-liposomes were prepared using co-loaded SLNs, the EE% of the hybrid system revealed that no drug loss occurred during the formulation, except for a tiny leakage of RIF (about 9%), probably due to the presence of ether during the preparation of the emulsion.

3.3. AFM analysis

A detailed AFM analysis was carried out to examine the morphological difference between the formulations. The morphology of unloaded SLNs, liposomes, and hybrid SLN-liposomes was assessed by AFM. As shown by the topographic images (Fig. 4), all the examined particles exhibited a spherical shape, confirming that the preparation of the hybrid system did not significantly affect the liposomal morphology. Phase images provided complementary information, revealing variations in certain surface properties of the nanocarriers, such as viscosity, elasticity, and viscoelasticity. These deviations are recorded by the probe, which detects phase signal changes, resulting from regions of different compositions. These phase shifts are visualized as bright and dark areas in the image, allowing the differentiation of materials. In detail, stiffer domains have a more positive phase shift, thus appearing as brighter than soft domains [21]. As can be noticed in the AMF images, the size of particles seems larger than that measured by PCS, especially for hybrid liposomes. This finding can be explained considering that AFM images can be affected by the movement of the cantilever probe, which, by pushing and warming the particles, determines a deformation of their original morphology [22].

3.4. SANS analysis

The SANS investigation was instrumental to the thorough characterization of the hybrid nanocarriers. In particular, it was useful to obtain further indications of the successful formation of the hybrid systems and to study the localization of the drugs in the particles.

Firstly, plain liposomes were investigated by SANS to obtain a fully characterized model for the comparative study of our hybrid systems (Fig. 5).

Liposome samples co-loaded with RIF and INH showed a slight increase in the lipid shell scattering length density (SLD, ρ_s) and a concomitant increment of the membrane thickness t, compared to unloaded liposomes (Table 2). This result was compatible with the encapsulation of the lipophilic RIF, which determines a rearrangement of the lipids in the single bilayer. A decrease in the SLD of the aqueous core, ascribable to the presence of INH, was also observed.

Subsequently, we characterized our new hybrid systems, unloaded and co-loaded with the two selected drugs. The outcomes of the SANS analysis are shown in Fig. 6, where they were compared with the data of the SLNs.

The dimensions of the unloaded hybrid SLN-liposomes (Table 3) were slightly bigger with respect to those of the corresponding unloaded liposomes (Table 2). This result may indicate the presence of the SLNs embedded in the core of the hybrid systems.

The analysis of the co-loaded hybrid SLN-liposome formulation also revealed a decrease in the SLD of the lipid shell (ρ_s) in the presence of INH and RIF (compared to the samples without SLN in Table 2). A comparative significant decrease in the SLD of the core (ρ_c) was observed for both unloaded and co-loaded hybrid SLN-liposomes, further indicating the encapsulation of SLNs in the aqueous core. More details about the shell and core SLD trends and their correlation with the drugs localization are reported in the discussion section.

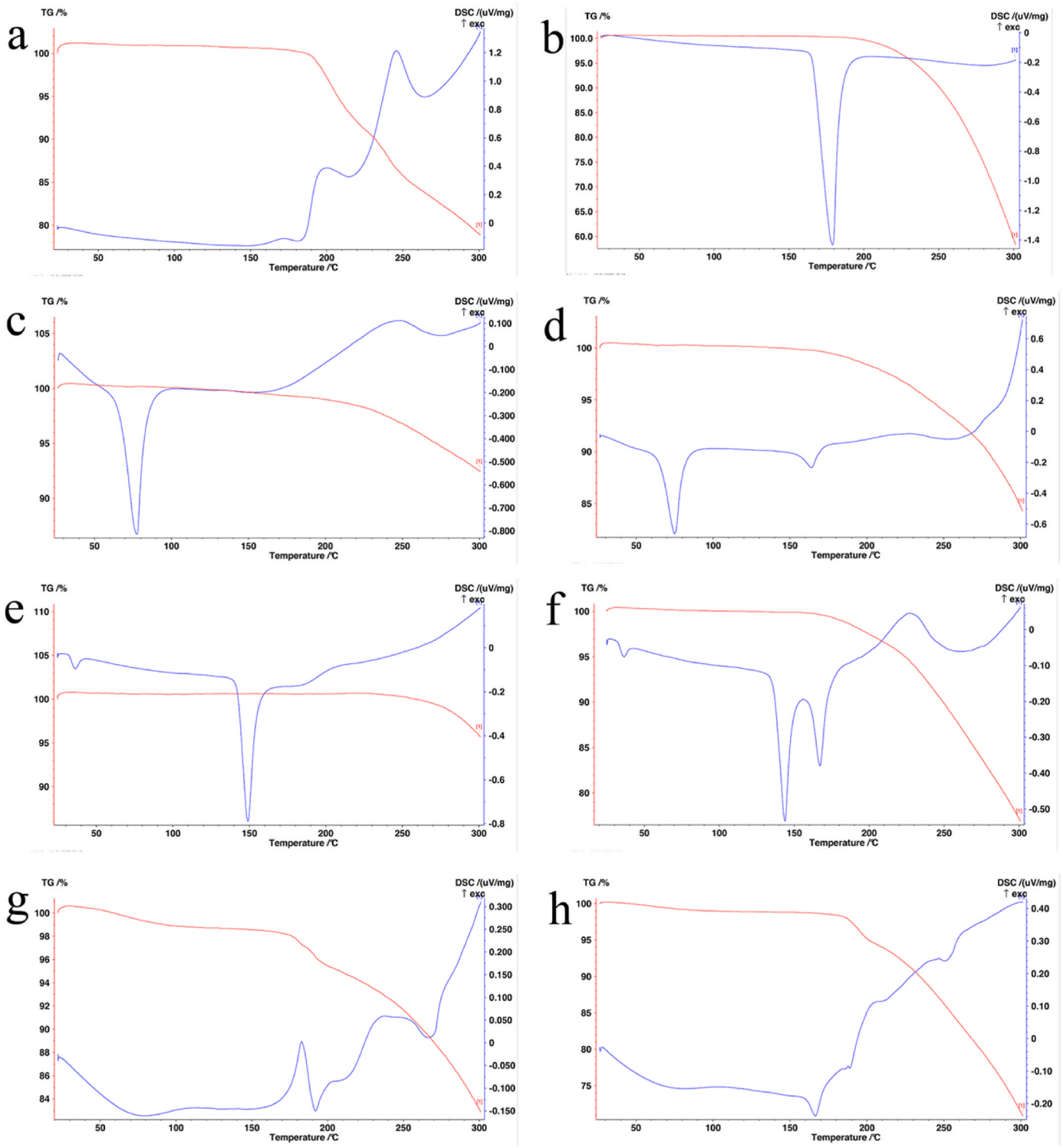

Fig. 3. Simultaneous thermogravimetry (red line) and differential scanning calorimetry (blue line) of RIF (a), INH (b), Compritol (c), compritol/drugs physical mixture (d), cholesterol (e), cholesterol/drugs physical mixture (f), lecithin (g), and lecithin/drugs physical mixture (h). (For interpretation of the references to color in this figure legend, the reader is referred to the Web version of this article.)

Notably, although the size of unloaded hybrid SLN-liposomes was comparable to that of unloaded plain liposomes, the dimensions of the co-loaded systems differ from each other by approximately 20 nm.

3.5. *In vitro* release study

To determine if these formulations exhibited different release kinetics, an *in vitro* release study was carried out, comparing the results to those obtained for the diffusion of the free drugs through a dialysis bag. All experiments were performed in triplicate in a time frame of 1–180 min, at 37 °C. The resulting kinetic profiles are depicted in Fig. 7.

Concerning the release curve of RIF, almost 25% of the drug was released from plain liposomes after 180 min. This value increased to 45% for the hybrid carriers. After a slight initial burst, like that of

Table 1
Size, PDI, Z-potential, EE% and DL% of SLN, liposomes and hybrid SLN-liposomes.

Formulation	Size (nm)	PDI	Z-potential (mV)	RIF		INH	
				EE %	DL% (w/w)	EE %	DL% (w/w)
Unloaded SLNs	122 ± 7	0.23 ± 0.01	−5.1 ± 11.9	/	/	/	/
Co-loaded plain SLNs	135 ± 9	0.25 ± 0.05	−25.3 ± 4.3	61.7 ± 3.9	10.3 ± 0.7[b]	31.3 ± 0.6[c]	5.2 ± 0.1[d]
Unloaded liposomes	300 ± 8	0.33 ± 0.02	−40.8 ± 5.4	/	/	/	/
Co-loaded plain liposomes	310 ± 7	0.30 ± 0.05	−51.5 ± 5.4	62.1 ± 4.9	8.1 ± 0.7[b]	46.9 ± 6.5[c]	6.1 ± 0.8[d]
Unloaded hybrid SLN-liposomes	343 ± 6	0.49 ± 0.04	−39.7 ± 5.2	/	/	/	/
Co-loaded hybrid SLN-liposomes	350 ± 9	0.45 ± 0.05	−40.8 ± 5.1	91.4 ± 0.2[a]	2.7 ± 0.1[b]	100 ± 0.2[a]	1.9 ± 0.1[d]

[a] EE% was calculated considering the actual loading of SLNs used in the formulation of the hybrid systems. DL% was calculated knowing the weight of SLNs in 3 mL of SLNs suspension added.
[b] $p < 0.01$ between SLNs and liposomes and $p < 0.001$ within hybrid SLN-liposomes and the other nanocarriers.
[c] $p < 0.01$ between SLNs and liposomes.
[d] $p < 0.01$ between SLNs and liposomes and $p < 0.001$ within hybrid SLN-liposomes and the other nanocarriers.

liposomes, the hybrid systems exhibited a release rate comparable to that of SLNs. This observation may indicate that the presence of the SLNs dictates the overall rate of the system; conversely, a slightly but significantly different profile was detected for plain liposomes.

Also for the hydrophilic IHN, huge differences in the release rate were observed: our data showed that SLNs released 100% of the drug in 3 h. On the contrary, the release from liposomes was slower: after a sharp burst effect, corresponding to 50% of INH released in 15 min, a plateau at 80% was reached, which lasted for the remainder of the experiment. Finally, hybrid SLN-liposomes released only 50% of the drug in 3 h, demonstrating an optimal ability to control the drug release.

4. Discussion

Due to their great advantages, SLNs are attracting the attention of researchers worldwide for their potential application in the pulmonary delivery of antitubercular drugs. However, one of the main drawbacks of SLNs is their inability to stably incorporate hydrophilic drugs [4,23]. In our previous work [9], liposomes proved to be suitable systems for the delivery of both hydrophilic and lipophilic drugs, such as INH and RIF, respectively.

In the present work, the development of a hybrid SLN-liposome system was attempted to design a novel strategy for a potential successful pulmonary delivery and controlled release of INH and RIF.

Considering the compatibility between drugs and excipients, the ATR-FTIR and the DSC analysis results suggested that the two drugs were compatible with the excipients employed in the formulation of SLN and liposomes [24].

The newly developed hybrid nanocarrier was compared to plain co-loaded SLNs and liposomes, in terms of size, morphology, structure, and *in vitro* release of both drugs.

Liposomes and hybrid SLN-liposome systems were formulated by using lecithin as a mixture of phospholipids to construct a bilayer shell, differently to our previous work, in which phosphatidylcholine (PC) was employed. Lecithin was preferred over PC in view of obtaining a therapeutic advantage for the management of TB. In addition to its surfactant properties, which are highly desirable for pulmonary medications, lecithin confers a negative charge to the liposomes, enhancing and sustaining the release of RIF in macrophages [25,26].

The characterization of the hybrid nanocarriers was initially performed by PCS, and the outcomes were compared to images obtained by AFM. From the PCS analysis, liposomes and hybrid SLN-liposomes displayed comparable particle sizes (~300 nm), while SLNs showed a smaller particle size (~130 nm), approximately half of that of liposomes. Despite the similar dimension, plain liposomes and hybrid systems differed for the particle homogeneity, as suggested by the increment of the PDI value, which increased from 0.3 to 0.45 in the case of the hybrid systems. The AFM images (Fig. 7) confirmed that the incorporation of the SLNs into the liposomes did not result in a significant size change with respect to plain liposomes. In AFM images, liposomes appeared as dark spots in the phase-images, due to their soft consistency; on the contrary, hybrid SLN-liposomes appear as light-colored structures, owing to the presence of smaller SLNs in the core with a stiffer domain. Moreover, the presence of small bright spots due to non-incorporated SLNs may explain the high PDI value recorded by PCS.

Concerning the drug loading investigation (Table 1), a high EE% was recorded for RIF in all the formulations, due to its hydrophobic interaction with the lipid matrix of SLNs and/or the lecithin bilayers of both liposomes and hybrid SLN-liposomes. As expected, RIF content in plain lecithin liposomes was lower than that of the PC-based liposomes of our previous work [9], despite they were prepared with the same formulation parameters. This difference can be attributable to the chemical nature of lecithin, which is composed of several phospholipids, including negatively charged phospholipids (e.g. phosphatidylinositol). It is known that in liposomes composed of phospholipids with negatively charged head groups, RIF localizes in a more superficial region, near the membrane interface, because of electrostatic repulsions between the anionic lipid and the ionized form of RIF [15]. Rodrigues et al. noticed that RIF can interact with various areas of the lipid bilayer with different partition coefficients, depending on the electrostatic/hydrophobic characteristics of the liposomes. In our case, plain lecithin liposomes showed a more negative Z-potential (−40.8 ± 5.4 mV) with respect to PC-liposomes (−20.5 ± 5.7 [27]), determining a repulsive electrostatic interference with RIF and concurring to its low incorporation. Moreover, the more negative charge of lecithin liposomes compared to PC liposomes also induced structural differences. For instance, the SANS scattering profile of the lecithin-based carriers did not exhibit the distinctive Bragg diffraction peak typical of multilamellar assemblies, suggesting a unilamellar structure, probably due to repulsive interaction between negative phospholipids [28]. Moreover, the size of liposomes co-loaded with INH and RIF differed from that of the hybrid formulations by about 20 nm. As previously observed in the case of multilamellar liposomes, the co-loading determines a stabilizing effect even in the case of unilamellar liposomes, coherent with the decrease in the liposome radius observed for liposomes in absence of SLN [9]. The presence of SLNs in the new hybrid systems might exert an analogous stabilizing effect, resulting in an overall similar behaviour.

Regarding the hybrid SLN-liposomes, the drug EE% was calculated by considering the drug loading in the SLNs employed in the formulation. Therefore, the EE of RIF (91.4%) suggested that part of the hydrophobic drug was lost during the preparation of the hybrid nanocarriers through the reverse-phase evaporation method. This minimal loss of RIF might be due to the organic solvent (ether) used to obtain the water-in-oil emulsion during the formulation process, which could extract RIF from the SLN lipid matrix. Besides providing invaluable information on the size and thickness of the drug carriers, the SANS analysis allowed to ascertain the presence of the drugs in the lipid structure. In accordance with the hypothesis formulated after the encapsulation analysis, evidence of the entrapment of RIF in the shell of the hybrid SLN-liposomes was revealed by an increase in the SLD of the

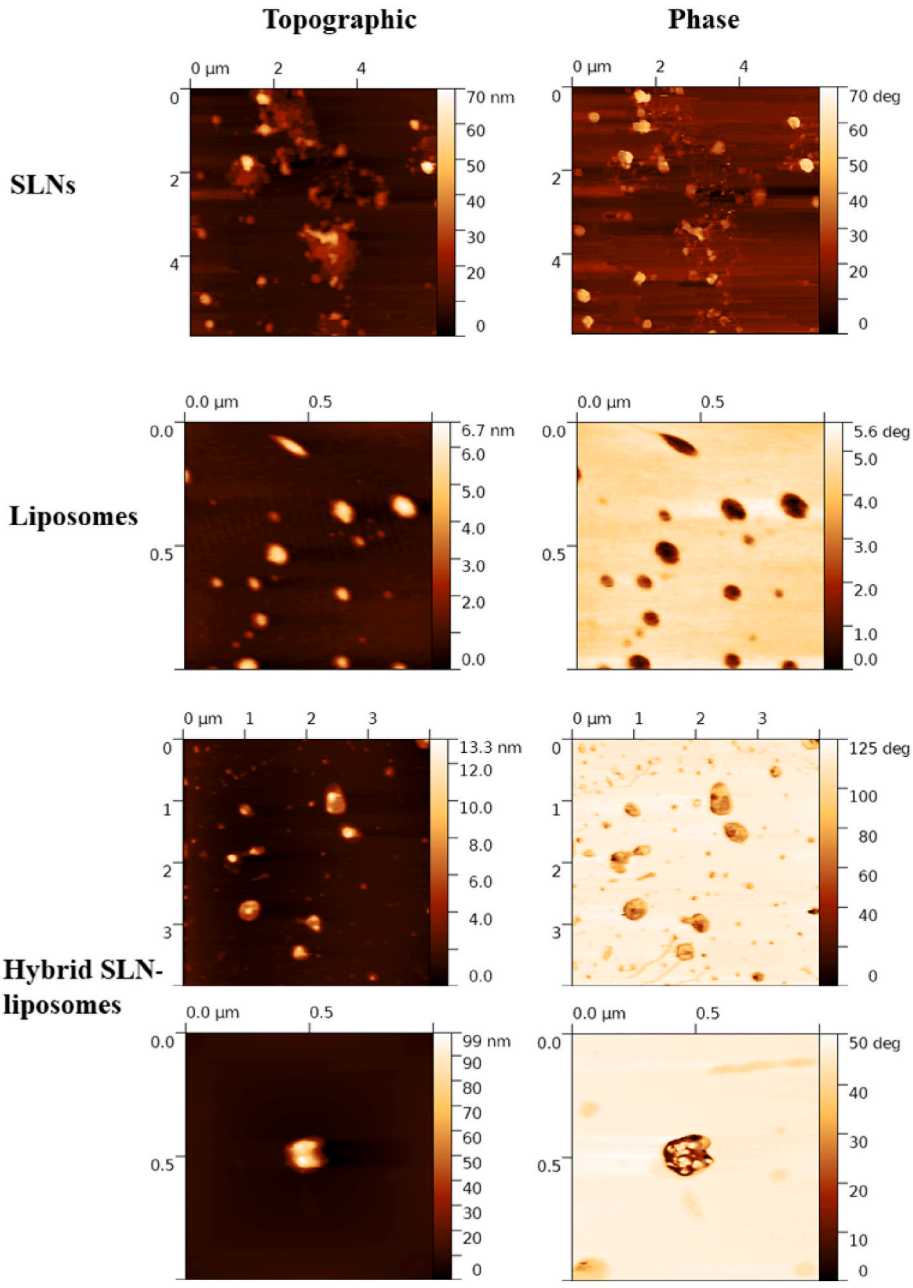

Fig. 4. Representative AFM images of SLNs, liposomes, and hybrid SLN-liposomes. The topographic images of the samples are depicted on the left, while the phase-signal images are on the right. The scale bars are present in the upper edge of each image.

lipid shell ($\rho_s = 3.01$) upon drug loading with respect to unloaded liposomes ($\rho_s = 2.95$). This effect is due to the inclusion of RIF molecules which, even in low quantities, induce a less dense, less compact, and more disordered packing of the lipid shell [9]. This might alter the stability of the lipid shell and even favor the release of RIF molecules in simulated lung fluid (SLF).

As far as the hydrophilic INH is concerned, SLNs demonstrated a lower EE% with respect to plain liposomes, due to the low dispersibility of the drug in the lipid matrix. The incorporation of SLNs in liposomes did not induce any loss of INH during the formulation process, as confirmed by the fact that hybrid SLN-liposomes displayed an EE% value near 100%. This evidence highlighted the superiority of our hybrid systems in obtaining a high incorporation efficiency, considering that both the drugs were successfully incorporated into the final hybrid nanosystem. This feature has been observed in other hybrid systems recently reported in the literature [29,30].

The release of RIF from all the nanocarriers was slower than the diffusion of the free drug through the dialysis bag (Fig. 7A), highlighting a sustained release pattern from all the lipid-based nanocarriers. The slower release of RIF may be attributable to the interaction with either the solid lipid matrix of SLNs or the hydrophobic tails of the liposomal bilayer, suggesting that in any case RIF was stably incorporated into the carriers [9,31]. *In vitro* sustained-release of RIF from hybrid SLN-liposomes was slightly higher than that observed for plain liposomes and SLNs. This difference could be due to the ether-induced extraction of RIF from the SLN matrix during the formulation process, as discussed in the encapsulation studies. The portion of RIF extracted during the water-in-oil emulsion preparation could be absorbed in the outer layer of the phospholipid shell. As shown by the release profiles depicted in Fig. 7, the highest percentage release of RIF was observed for the hybrid systems (which retained more of it in terms of EE%, both in the core and in the shell), followed by SLNs (only in the core), and

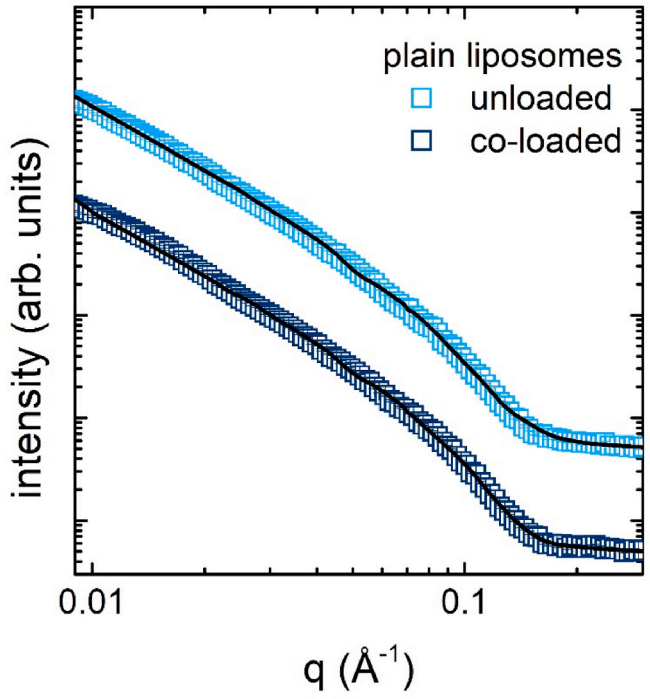

Fig. 5. SANS scattering profile of plain liposomes: unloaded liposomes dispersed in D_2O (light blue squares) and co-loaded liposomes with both INH and RIF dispersed in D_2O (dark blue points). Best fits (solid lines) are reported in black. The curves are vertically shifted to better visualize the differences between the trends. (For interpretation of the references to color in this figure legend, the reader is referred to the Web version of this article.)

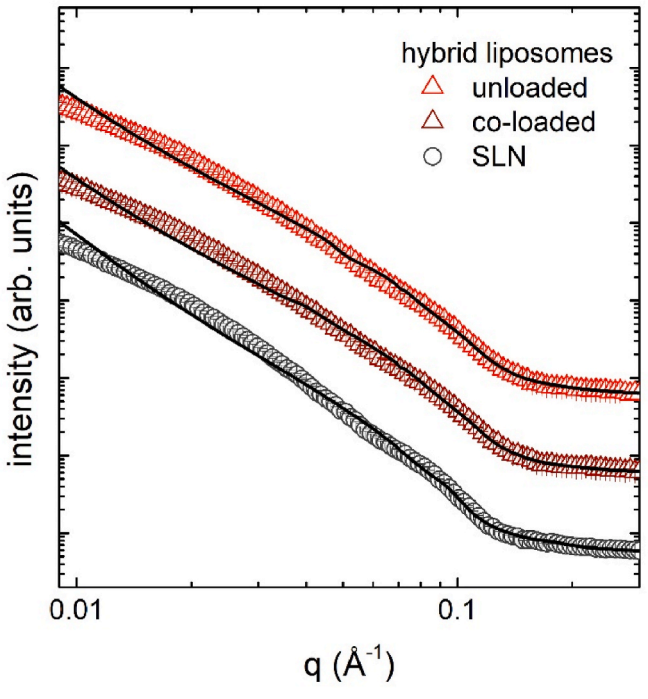

Fig. 6. SANS scattering profile of SLNs and hybrid liposomes: SLNs (grey circles), unloaded hybrid liposomes (orange triangles), and co-loaded hybrid liposomes with both INH and RIF (red triangles). Best fits (solid lines) are reported in black. The curves are vertically shifted to better visualize the differences between the trends. (For interpretation of the references to color in this figure legend, the reader is referred to the Web version of this article.)

Table 2
Fit parameters for plain liposomes: ρ_c, SLD of the core; ρ_s, SLD of the shell, r_c, radius of the core; t, thickness of the shell.

Formulation	ρ_c [$\cdot 10^{-6}$ Å^{-2}]	ρ_s [$\cdot 10^{-6}$ Å^{-2}]	r_c (nm)[a]	t (nm)[a]	size (nm)
Unloaded liposomes	6.40	2.97	202 ± 1 [0.3]	3.3 ± 0.1 [0.3]	410 ± 2
Co-loaded liposomes	6.38	3.48	197 ± 1 [0.3]	3.5 ± 0.1 [0.2]	401 ± 2

[a] The corresponding polydispersity values assuming a Gaussian distribution are reported in square brackets.

liposomes (only in the shell).

Diffusion of free INH across the dialysis membrane indicated that the entire drug was dissolved in <60 min (Fig. 7B). SLNs slowly released the drug with quite a linear profile, reaching 100% in 4 h. On the contrary, liposomes, being a vesicular system, released the hydrophilic drug with a profile similar to that of the free drug, probably due to the high permeability of the unilamellar liposomal membrane [32]. Hybrid SLN-liposomes showed a typical biphasic release profile, with a burst release in the first 30 min followed by a sustained release in the next 3 h. The decrease in the SLD of the core of hybrid liposomes witnesses the incorporation of INH and SLNs, with a high EE%. The two compounds indeed show SLDs that are lower compared to that of D2O, due to their molecular composition. Hence, INH was trapped in the SLNs embedded in the core of the hybrid systems, which enhanced its retention in SLF with respect to plain liposomes, resulting in a unique release profile. In agreement with previous data [33], this finding suggested that hybrid systems have the potential to delay the release of inhaled drugs from different matrices due to the presence of a diffusional barrier on the nanoparticle surface.

Table 3
Fit parameters for SLNs and hybrid liposomes: ρ_c, SLD of the core; ρ_s, SLD of the shell, r_c, radius of the core; t, thickness of the shell.

Formulation	ρ_c [$\cdot 10^{-6}$ Å^{-2}]	ρ_s [$\cdot 10^{-6}$ Å^{-2}]	r_c (nm)[a]	t (nm)[a]	size (nm)
Unloaded SLNs	0.59	−2.17	66 ± 1 [0.3]	4.3 ± 0.5 [0.3]	140 ± 4
Unloaded hybrid SLN-liposomes	5.11	2.95	203 ± 2 [0.2]	3.9 ± 0.2 [0.3]	414 ± 6
Co-loaded hybrid SLN-liposomes	5.15	3.01	206 ± 2 [0.2]	3.8 ± 0.1 [0.3]	419 ± 6

[a] The corresponding polydispersity values assuming a Gaussian distribution are reported in square brackets.

5. Conclusions

The present investigation highlights the prospects of nanoscale shell-core SLN-liposome hybrids as efficient carriers for a potential pulmonary delivery of antitubercular drugs. This formulation prevents the leakage of small hydrophilic compounds and increases the entrapment of drugs. These novel systems were able to release their content as expected from a successful dosage form for inhaled administration, improving the stability and the drug release profile with respect to plain liposomes. The physicochemical characterization of our systems opens new avenues towards a better understanding of the formulation of vesicles encapsulating SLNs. The SANS analysis allowed us to precisely define the variation in size of the nanosystems after the encapsulation of co-loaded SLNs The *in vitro* dissolution studies depicted an initial burst release followed by a sustained release profile, significantly slower compared to that of plain liposomes.

We can conclude that the hybrid system designed and characterized in this work offers various benefits with respect to conventional nanocarriers, such as a high encapsulation efficiency, a controlled particle

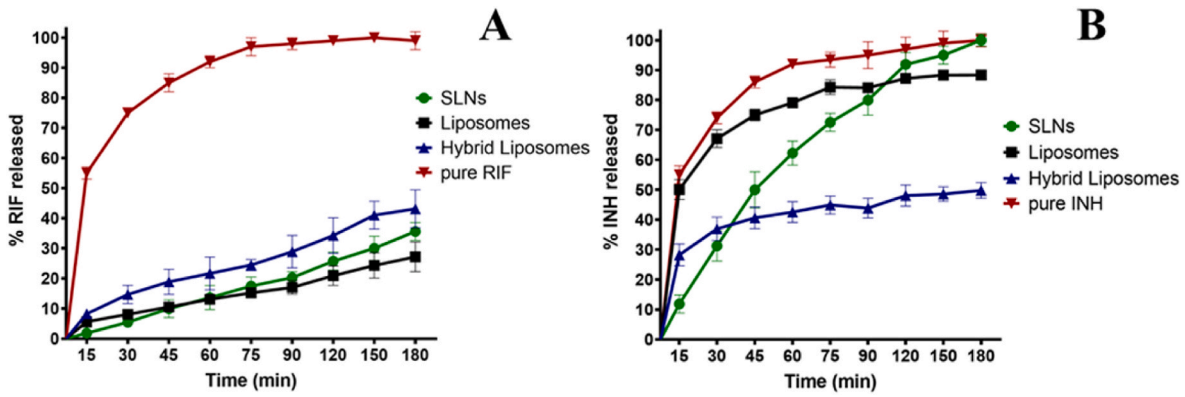

Fig. 7. *In vitro* release of RIF (A) and INH (B) from co-loaded SLNs, liposomes, and hybrid SLN-liposomes.

size, and the potential to load multiple therapeutic agents, determining a prolonged release of the drug. Respirability parameters as well as biological studies *in vitro* and *in vivo* will be planned to confirm the advantages of this hybrid SLN-liposomal system in the treatment of lung infections.

Author statement file

E. Leo, F. Domenici, and C. Castellano conceptualization and supervision; E. Truzzi, A. Capocefalo and C. Castellano: investigation and formal analysis; E. Truzzi, M. Mori and E. Maretti: methodology and data curation. A. Capocefalo and F. Domenici: Software; E. Leo and F. Meneghetti writing original draft; F. Domenici, and V. Iannuccelli: Writing - review & editing. E. Leo, F. Meneghetti, C. Castellano and F. Domenici: funding acquisition.

All authors have read and agreed to the published version of the manuscript.

Declaration of competing interest

Authors E. Truzzi, A. Capocefalo, E. Maretti, M. Mori, V. Iannuccelli, F. Domenici, C. Castellano and E. Leo declare that they have no conflict of interest.

Acknowledgements

Authors thank Dr. B. Kent for assistance during the SANS experiment and Dr. Paola Miselli (University of Modena and Reggio Emilia) for the DSC analysis. The research leading to SANS results has been supported by BER II at HZB under the Grant Agreement n.17205592-ST.

This work was financially supported by the University of Modena and Reggio Emilia, (FAR2019-DSV-Leo) and the University of Milan (Linea B). This work also benefited from the use of the SasView application, originally developed under NSF Award DMR-0520547. SasView also contains code developed with funding from the EU Horizon 2020 program under the SINE2020 project Grant No 654000.

Appendix A. Supplementary data

Supplementary data to this article can be found online at https://doi.org/10.1016/j.jddst.2022.103206.

References

[1] C. Weiss, M. Carriere, L. Fusco, L. Fusco, I. Capua, J.A. Regla-Nava, M. Pasquali, M. Pasquali, M. Pasquali, J.A. Scott, F. Vitale, F. Vitale, M.A. Unal, C. Mattevi, D. Bedognetti, A. Merkoçi, A. Merkoçi, E. Tasciotti, E. Tasciotti, A. Yilmazer, A. Yilmazer, Y. Gogotsi, F. Stellacci, F. Stellacci, L.G. Delogu, Toward nanotechnology-enabled approaches against the COVID-19 pandemic, ACS Nano 14 (2020) 6383–6406, https://doi.org/10.1021/acsnano.0c03697.

[2] A.A. Yetisgin, S. Cetinel, M. Zuvin, A. Kosar, O. Kutlu, Therapeutic nanoparticles and their targeted delivery applications, Molecules 25 (2020) 2193, https://doi.org/10.3390/molecules25092193.

[3] C.L. Ngan, A.A. Asmawi, Lipid-based pulmonary delivery system: a review and future considerations of formulation strategies and limitations, Drug Deliv. Transl. Res. 8 (2018) 1527–1544, https://doi.org/10.1007/s13346-018-0550-4.

[4] R. Paliwal, S.R. Paliwal, R. Kenwat, B. Das Kurmi, M.K. Sahu, Solid lipid nanoparticles: a review on recent perspectives and patents, Expert Opin. Ther. Pat. 30 (2020) 179–194, https://doi.org/10.1080/13543776.2020.1720649.

[5] E. Maretti, C. Rustichelli, M.L. Gualtieri, L. Costantino, C. Siligardi, P. Miselli, F. Buttini, M. Montecchi, E. Leo, E. Truzzi, V. Iannuccelli, The impact of lipid corona on rifampicin intramacrophagic transport using inhaled solid lipid nanoparticles surface-decorated with a mannosylated surfactant, Pharmaceutics 11 (2019) 508, https://doi.org/10.3390/pharmaceutics11100508.

[6] E. Truzzi, T.L. Nascimento, V. Iannuccelli, L. Costantino, E.M. Lima, E. Leo, C. Siligardi, M.L. Gualtieri, E. Maretti, In vivo biodistribution of respirable solid lipid nanoparticles surface-decorated with a mannose-based surfactant: a promising tool for pulmonary tuberculosis treatment? Nanomaterials 10 (2020) 1–15, https://doi.org/10.3390/nano10030568.

[7] E. Maretti, L. Costantino, F. Buttini, C. Rustichelli, E. Leo, E. Truzzi, V. Iannuccelli, Newly synthesized surfactants for surface mannosylation of respirable SLN assemblies to target macrophages in tuberculosis therapy, Drug Deliv. Transl. Res. 9 (2019) 298–310, https://doi.org/10.1007/s13346-018-00607-w.

[8] E. Nemati, A. Mokhtarzadeh, V. Panahi-Azar, A. Mohammadi, H. Hamishehkar, M. Mesgari-Abbasi, J. Ezzati Nazhad Dolatabadi, M. de la Guardia, Ethambutol-loaded solid lipid nanoparticles as dry powder inhalable formulation for tuberculosis therapy, AAPS PharmSciTech 20 (2019), https://doi.org/10.1208/s12249-019-1334-y.

[9] E. Truzzi, F. Meneghetti, M. Mori, L. Costantino, V. Iannuccelli, E. Maretti, F. Domenici, C. Castellano, S. Rogers, A. Capocefalo, E. Leo, Drugs/lamellae interface influences the inner structure of double-loaded liposomes for inhaled anti-TB therapy: an in-depth small-angle neutron scattering investigation, J. Colloid Interface Sci. 541 (2019) 399–406, https://doi.org/10.1016/j.jcis.2019.01.094.

[10] M. Rudokas, M. Najlah, M.A. Alhnan, A. Elhissi, Liposome delivery systems for inhalation: a critical review highlighting formulation issues and anticancer applications, Med. Princ. Pract. 25 (2016) 60–72, https://doi.org/10.1159/000445116.

[11] D. Cipolla, I. Gonda, H. Chan, Liposomal formulations for inhalation, Ther. Deliv. 4 (2013) 1047–1072, https://doi.org/10.4155/tde.13.71.

[12] J.F. García-Rodríguez, N. Valcarce-Pardeiro, H. Álvarez-Díaz, A. Mariño-Callejo, Long-term efficacy of 6-month therapy with isoniazid and rifampin compared with isoniazid, rifampin, and pyrazinamide treatment for pleural tuberculosis, Eur. J. Clin. Microbiol. Infect. Dis. 38 (2019) 2121–2126, https://doi.org/10.1007/s10096-019-03651-7.

[13] J. Costa-Gouveia, E. Pancani, S. Jouny, A. Machelart, V. Delorme, G. Salzano, R. Iantomasi, C. Piveteau, C.J. Queval, O.-R. Song, M. Flipo, B. Deprez, J.-P. Saint-André, J. Hureaux, L. Majlessi, N. Willand, A. Baulard, P. Brodin, R. Gref, Combination therapy for tuberculosis treatment: pulmonary administration of ethionamide and booster co-loaded nanoparticles, Sci. Rep. 7 (2017) 5390, https://doi.org/10.1038/s41598-017-05453-3.

[14] M. Tilinca, G. Hancu, E. Mircia, D. Iriminescu, A. Rusu, R.A. Vlad, E. Barabás, Simultaneous determination of isoniazid and rifampicin by UV spectrophotometry, FARMACIA 65 (2017) 219–224.

[15] A. Gürsoy, E. Kut, S. Özkirimli, Co-encapsulation of isoniazid and rifampicin in liposomes and characterization of liposomes by derivative spectroscopy, Int. J. Pharm. 271 (2004) 115–123, https://doi.org/10.1016/j.ijpharm.2003.10.033.

[16] O. Arnold, J.C. Bilheux, J.M. Borreguero, A. Buts, S.I. Campbell, L. Chapon, M. Doucet, N. Draper, R. Ferraz Leal, M.A. Gigg, V.E. Lynch, A. Markvardsen, D. J. Mikkelson, R.L. Mikkelson, R. Miller, K. Palmen, P. Parker, G. Passos, T. G. Perring, P.F. Peterson, S. Ren, M.A. Reuter, A.T. Savici, J.W. Taylor, R.J. Taylor, R. Tolchenov, W. Zhou, J. Zikovsky, Mantid - data analysis and visualization package for neutron scattering and μ SR experiments, Nucl. Instruments Methods

Phys. Res. Sect. A Accel. Spectrometers, Detect. Assoc. Equip. 764 (2014) 156–166, https://doi.org/10.1016/j.nima.2014.07.029.
[17] A. Guinier, G. Fournet, C.B. Walker, G.H. Vineyard, Small-angle scattering of X-rays, Phys. Today 9 (1956) 38–39, https://doi.org/10.1063/1.3060069.
[18] M.R.C. Marques, R. Loebenberg, M. Almukainzi, Simulated biological fluids with possible application in dissolution testing, Dissolution Technol. 18 (2011) 15–28, https://doi.org/10.14227/DT180311P15.
[19] J. Coates, Interpretation of infrared spectra, A practical approach, Encycl. Anal. Chem. 1 (2006) 1–23, https://doi.org/10.1002/9780470027318.a5606.
[20] M. Singh, A. Guzman-Aranguez, A. Hussain, C.S. Srinivas, I.P. Kaur, Solid Lipid Nanoparticles for Ocular Delivery of Isoniazid: Evaluation, Proof of Concept and in Vivo Safety & Kinetics, https://doi.org/10.2217/Nnm-2018-0278. 14 (2019) 465–491. doi:10.2217/NNM-2018-0278.
[21] S.N. Magonov, V. Elings, M.H. Whangbo, Phase imaging and stiffness in tapping-mode atomic force microscopy, Surf. Sci. 375 (1997) L385–L391, https://doi.org/10.1016/S0039-6028(96)01591-9.
[22] E. Vighi, B. Ruozi, M. Montanari, R. Battini, E. Leo, Re-dispersible cationic solid lipid nanoparticles (SLNs) freeze-dried without cryoprotectors: characterization and ability to bind the pEGFP-plasmid, Eur. J. Pharm. Biopharm. 67 (2007) 320–328, https://doi.org/10.1016/j.ejpb.2007.02.006.
[23] E. Vighi, M. Montanari, M. Hanuskova, V. Iannuccelli, G. Coppi, E. Leo, Design flexibility influencing the in vitro behavior of cationic SLN as a nonviral gene vector, Int. J. Pharm. 440 (2013) 161–169, https://doi.org/10.1016/j.ijpharm.2012.08.055.
[24] F. Ali, R. Kumar, P.L. Sahu, G.N. Singh, Physicochemical characterization and compatibility study of roflumilast with various pharmaceutical excipients, J. Therm. Anal. Calorim. 1303 (130) (2017) 1627–1641, https://doi.org/10.1007/S10973-017-6274-8, 2017.
[25] G. Chimote, R. Banerjee, In vitro evaluation of inhalable isoniazid-loaded surfactant liposomes as an adjunct therapy in pulmonary tuberculosis, J. Biomed. Mater. Res. B Appl. Biomater. 94 (2010) 1–10, https://doi.org/10.1002/jbm.b.31608.
[26] S.P. Vyas, M.E. Kannan, S. Jain, V. Mishra, P. Singh, Design of liposomal aerosols for improved delivery of rifampicin to alveolar macrophages, Int. J. Pharm. 269 (2004) 37–49, https://doi.org/10.1016/j.ijpharm.2003.08.017.
[27] F. Sacchetti, D. D'Arca, F. Genovese, S. Pacifico, E. Maretti, M. Hanuskova, V. Iannuccelli, M.P. Costi, E. Leo, Conveying a newly designed hydrophilic anti-human thymidylate synthase peptide to *cisplatin* resistant cancer cells: are pH-sensitive liposomes more effective than conventional ones? Drug Dev. Ind. Pharm. 43 (2017) 465–473, https://doi.org/10.1080/03639045.2016.1262870.
[28] C.I. Nkanga, R.W. Krause, X.S. Noundou, R.B. Walker, Preparation and characterization of isoniazid-loaded crude soybean lecithin liposomes, Int. J. Pharm. 526 (2017) 466–473, https://doi.org/10.1016/j.ijpharm.2017.04.074.
[29] E. Maretti, B. Pavan, C. Rustichelli, M. Montanari, A. Dalpiaz, V. Iannuccelli, E. Leo, Chitosan/heparin polyelectrolyte complexes as ion-paring approach to encapsulate heparin in orally administrable SLN: in vitro evaluation, Colloids Surfaces A Physicochem. Eng. Asp. 608 (2021), 125606, https://doi.org/10.1016/j.colsurfa.2020.125606.
[30] A. Wünsch, D. Mulac, K. Langer, Lecithin coating as universal stabilization and functionalization strategy for nanosized drug carriers to overcome the blood–brain barrier, Int. J. Pharm. 593 (2021), https://doi.org/10.1016/j.ijpharm.2020.120146.
[31] C. Rodrigues, P. Gameiro, M. Prieto, B. De Castro, Interaction of rifampicin and isoniazid with large unilamellar liposomes: spectroscopic location studies, Biochim. Biophys. Acta Gen. Subj. 1620 (2003) 151–159, https://doi.org/10.1016/S0304-4165(02)00528-7.
[32] A. Jain, S.K. Jain, In vitro release kinetics model fitting of liposomes: an insight, Chem. Phys. Lipids 201 (2016) 28–40, https://doi.org/10.1016/j.chemphyslip.2016.10.005.
[33] F. Mottaghitalab, M. Farokhi, Y. Fatahi, F. Atyabi, R. Dinarvand, New insights into designing hybrid nanoparticles for lung cancer: diagnosis and treatment, J. Contr. Release 295 (2019) 250–267, https://doi.org/10.1016/j.jconrel.2019.01.009.